Accepted Manuscript

Effect of perlite particle contents on delamination toughness of S-glass fiber reinforced epoxy matrix composites

Mohamad Alsaadi, Ahmet Erkliğ

PII: S1359-8368(16)31732-2

DOI: 10.1016/j.compositesb.2017.12.059

Reference: JCOMB 5488

To appear in: *Composites Part B*

Received Date: 25 August 2016

Revised Date: 2 November 2017

Accepted Date: 29 December 2017

Please cite this article as: Alsaadi M, Erkliğ A, Effect of perlite particle contents on delamination toughness of S-glass fiber reinforced epoxy matrix composites, *Composites Part B* (2018), doi: 10.1016/j.compositesb.2017.12.059.

Effect of perlite particle contents on delamination toughness of S-glass fiber reinforced epoxy matrix composites

Mohamad Alsaadi[1,2], Ahmet Erkliğ[1]
[1]*Gaziantep University, Faculty of Engineering, Mechanical Engineering Department/ Gaziantep 27310, Turkey*
[2]*University of Technology, Materials Engineering Department/Baghdad 10066, Iraq*
mohamad.alsaadi@mail2.gantep.edu.tr, phd.mohamadalsaadi@gmail.com

ABSTRACT

The effects of perlite particulate-filler on the mode I and mode II interlaminar fracture and mechanical behavior of glass fabric/epoxy composites were studied. Composite specimens for double-cantilever beam (DCB), end-notched flexure (ENF) tensile and flexural tests were prepared and tested according to ASTM standards with perlite contents of 1, 3, 5 and 10 wt%. The optical and scanning electron microscopes images were described the mechanisms of mode I and II interlaminar fracture. The results indicated that the mode I and mode II interlaminar fracture toughness were optimum at perlite content of 3 wt% with increment of 39.9% and 72.3%, respectively. The tensile strength and flexural properties reached maximum values at perlite content of 1 and 5 wt%, respectively.

*Keywords***:** Perlite; Glass fiber; Epoxy; Mechanical properties; Interlaminar fracture; Delamination.

1. Introduction

The preferred properties and useful characteristics of glass fibers reinforced polymer (GFRP) composites like high modulus, strength, good impact resistance and high resistance to environmental make suitable for many applications such as piping, automobile, aircraft and marine industries [1-2]. Nevertheless, GFRP has poor resistance to delamination [3]. This issue may be ascribed to the lack of fibers reinforcement oriented in the laminate depth for effective transverse of the applied force that can be circumvented by Z-fiber stitching or pinning other fibers to join layers [4-6]. However, tensile properties of composites reduce by this technique and need other manufacturing procedures [7, 8]. Epoxy resins have been usually used in GFRP laminates for above applications due to low shrinkage during curing, high corrosion resistance and working capability under various conditions [9]. Therefore, researchers used high performance epoxy like dendritic hyperbranched to improve delamination toughness, but its needs more improving [10]. The other toughing method is including particulate-filler within laminate composite, which some researchers used thermoplastics and rubber fillers [11, 12]. However, when high molecular weight of thermoplastics and rubber particles are incorporated, the epoxy viscosity is raised and lead to difficulties in composite lamination process. Although the interlaminar fracture toughness is usually elevated with previous technique, the stiffness and strength are reduced.

The rigid inorganic micro- and nano-particles have been used in fabrication of composite laminates in recent years due to improving the composites mechanical properties and interlaminar fracture [13-33]. In addition, some waste and cheap fillers can reduce the cost of fabrication and product [34].

Wang et al. [13] used Al_2O_3 micro-particles to raise flexural strength, impact strength and mode II interlaminar toughness by 16%, 37% and 50.0%, respectively, for carbon fiber reinforced epoxy composite. Wang et al. [17] examined nano-whiskers to increase mode I interlaminar toughness of the composite from 140 J/m^2 to 220 J/m^2. Jen et al. [20] improved PEEK/AS-4 composite strength by 12% with addition 1 wt% of nano-silica particles. Kumar and Roy [30] employed nanographene particles to enhance mode I and mode II interlaminar fracture toughness of carbon fiber reinforced epoxy composite. The resistance to crack propagation was significantly improved with incorporation nanographene platelets of 0.5 wt%. Therefore, according to the previous researches, the addition of inorganic rigid particles may increase the mechanical properties in addition to mode I and mode II interlaminar fracture toughness. Thus, it is essential to investigate the influence of particle content, particularly cheap particulate fillers, on the delamination resistance of composite laminates to be more clarified.

Perlite is a natural white color inorganic mineral material, based on silicon dioxide and it is characterized by low cost, lightly weight, porous structure, insulating, non-explosive, high strength and has thermal, biological and chemical stability. Therefore, perlite has variety of applications such as refractory block, high thermal insulation, filtration, and filler for various composites types [35, 36]. However, there is a little attention to use perlite as modifying filler in composite structure. Researches were indicated improvements in the tensile and impact strength with addition of perlite within polymer composites [37-40]. Shastri and Kim [41] studied the effect of expanded perlite particles on the compressive strengths and modulus of the fabricated perlite foams as construction material applications.

According to the above literature survey, many of these studies are related to interlaminar toughness and mechanical properties by using a variety of micro- and nano-particle filled composites. To the best knowledge of the authors, researchers in literature do not adequately investigate the influence of perlite filler content on interlaminar fracture toughness of GFRP. The goal of this article was to investigate the effect of perlite (Pr) content on the interlaminar fracture toughness for mode I and mode II deformation, tensile strength and flexural properties of glass fiber reinforced epoxy (GFRE) composites. In addition to investigate the interlaminar fracture behavior for each composite laminate, the forms of failure and deformation were examined using scanning electron and optical microscopes, in order to present toughening mechanism of each composite laminate.

2. Materials and procedures

2.1. Materials

To prepare the particulate-filled composite laminates, woven plain S-glass fibers with areal density of 200 g/m^2 were used as reinforcement in the laminated composites. Epoxy (MOMENTIVE-MGS L285) with hardener (MOMENTIVE-MGS H285) were blended in a stoichiometric weight ratio of 100/40. Production materials were provided from DOST Chemical Industrial Raw Materials Industry, Turkey. The filler of Perlite was supplied by Inper Perlite, Gaziantep, Turkey. The particle size was measured approximately 1-35 µm for grinded and garbled Pr particles. The bulk densities of Pr was measured equal to 0.16 gr/cm^3 and the chemical compositions are given in Table 1.

Table 1
Chemical Compositions of perlite.

Filler	Chemical formula/Composition wt%
Perlite	SiO_2 (71-75), AlO_3 (12.5-18), Na_2O_3 (2.9-4), K_2O (0.5-5), Fe_2O_3 (0.1-0.5), MgO (0.02-0.5), TiO_2 (0.03-0.2), SO_3 (0-0.2).

2.2. Laminates fabrication and specimens preparation

The grinded of perlite filler was garbled by sieving to get fine particles in the range of 1-35 µm. The composites were prepared by adding perlite particles in epoxy resin with four different contents 1, 3, 5 and 10 wt%. The measured quantity of the perlite was added gradually in the epoxy resin and mixed it evenly by using a mechanical stirrer with a constant speed of 750 RPM for 25 minutes in order to obtain a homogeneous mixture. Then hardener was added to the mixture for quick setting of laminate composite. Laminated fabrics were manufactured by the application of the resin mixture to the fibers layer by layer at room temperature (25°C). This process is repeated till all the 16 layers were placed. A heat-resistant Teflon film with thickness of 12 µm was inserted at mid-plane along one edge of the laminate during hand lay-up process in order to introduce a starter crack for DCB and ENF specimens. Then, modified laminated fabrics with dimensions of 240 mm × 300 mm were applied to 0.3 MPa pressure between two flat molds with 80 ^{o}C temperature for 1 h curing time. Afterward, laminate were cooled to the room temperature under the pressure (Process of laminate production is shown in Fig. 1). After the production of composite laminates tensile, flexural, DCB and ENF specimens (Fig. 2) were cut according to ASTM standards.

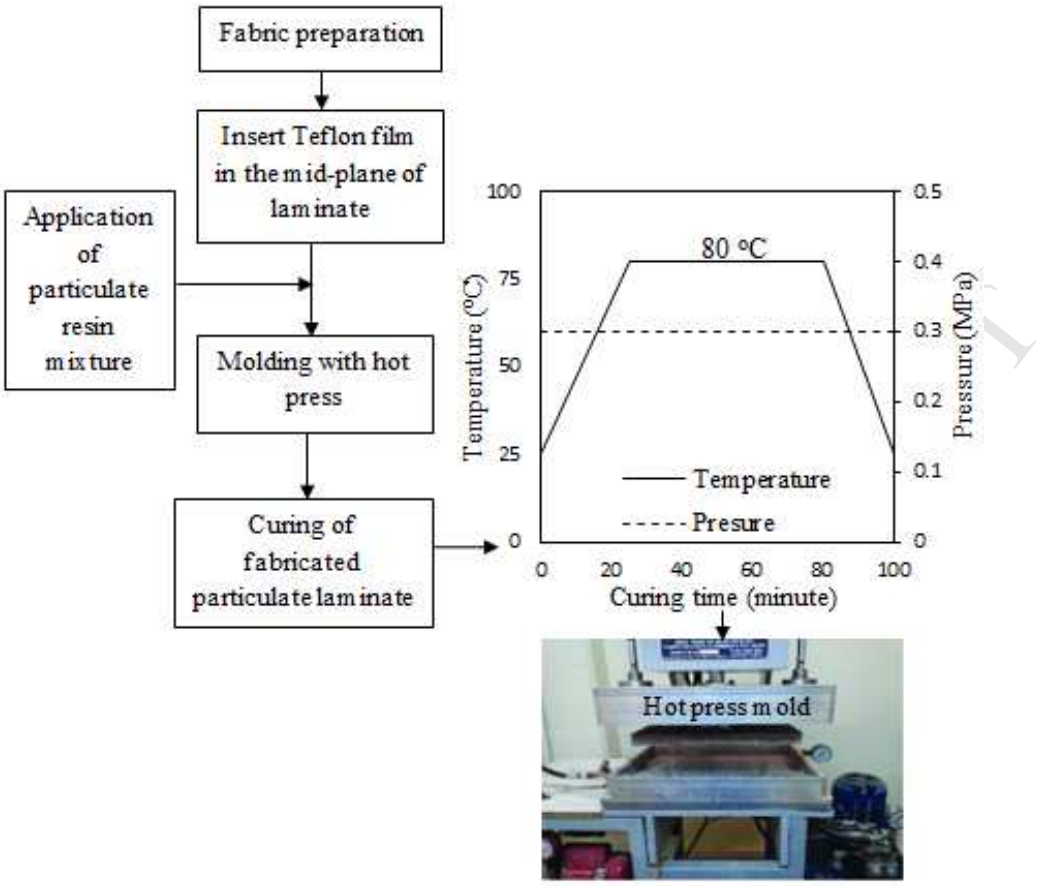

Fig. 1. Production process and unit.

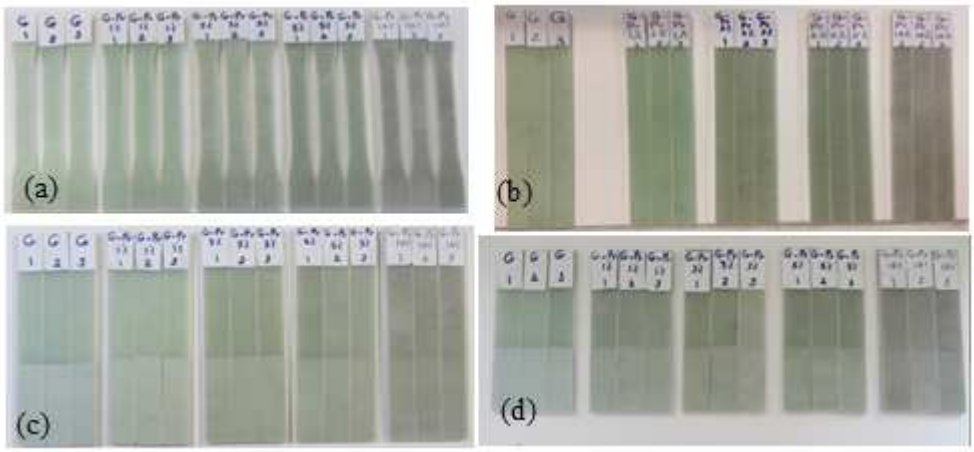

Fig. 2. Specimens of Pr-GFRE composites for: (a) tensile (b) flexural (c) DCB and (d) ENF tests.

2.3. Testing procedures

2.3.1. Mode I testing

The interlaminar fracture toughness under mode I and mode II loadings and mechanical properties of the composites were determined using the Shimadzu tensile testing machine AG-X series (Kyoto, Japan) at room temperature. Strain energy

release rate (G) represents the resistance to delamination growth, which the interlaminar fracture toughness is a measured value for the critical energy release rate (G_C). The mode I interlaminar fracture toughness (G_{IC}) of the GFRE and the Pr-GFRE composites were evaluated using the DCB test according to the ASTM D 5528 standard [42]. The specimens of DCB test were cut in the dimensions of 165×20 mm. Aluminum loading blocks measuring 20×25×12 mm with a loading hole of 6 mm diameter were stuck to each side on the cracked end of DCB specimens by using Araldite 2014 adhesive. The pre-crack length (a_o) was 50 mm according to the inserted Teflon film. Fig. 3 shows the configuration of DCB test specimen and a picture for specimen during testing. The crosshead displacement in the DCB test was explained as crack opening displacement (COD) of the specimen. The crack propagation length were recorded using a digital camera. The crosshead speed of DCB tests was 5 mm/min in accordance with ASTM D 5528. The data of DCB test were recorded in term of P-COD and corresponding P-a values, where a and P refer to crack extension length and load applied at which the crack grows, respectively. The mode I interlaminar fracture toughness (G_{IC}) is determined by using the general formula from linear elastic fracture mechanics [3]:

$$G_{IC} = \frac{P^2}{2b}\frac{\partial C}{\partial a} = \frac{P\delta}{2bC}\frac{\partial C}{\partial a} \quad (1)$$

Where b is the specimen width, δ is the COD and C is the compliance. By differentiating the compliance C, which C is equal to δ/P, and substitution into equations 1 to get:

$$G_{IC} = \frac{3P\delta}{2ba} \quad (2)$$

In reality, this expression overestimates G_{IC} values because the equation above is valid only for the perfectly built-in cantilever beam. In practice, the DCB is not perfectly built-in, therefore corrections are needed for shear deformation, rotation at the crack tip and large displacements. Some of these effects may be treated by correcting the crack length, that becomes slightly longer, a+|Δ|, where the crack length correction, Δ may be found by plotting cube root of the compliance, $C^{1/3}$, as a function of the crack extension length. The mode I interlaminar toughness now becomes [3, 43-46]:

$$G_{IC} = \frac{3P\delta}{2b(a+|\Delta|)} \quad (3)$$

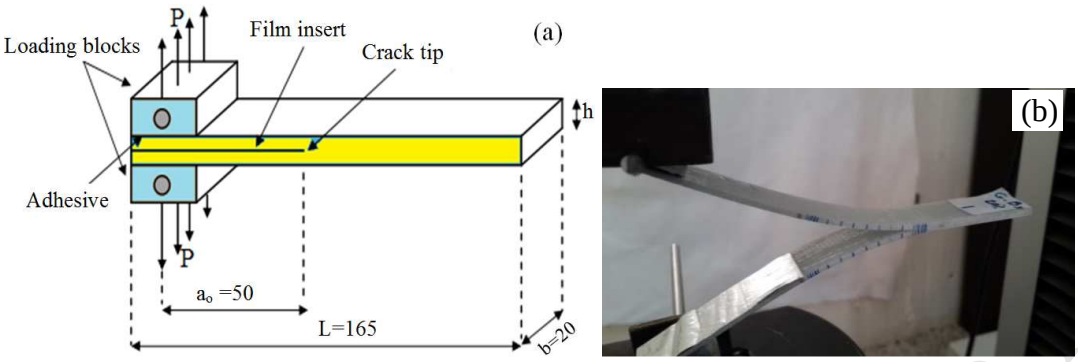

Fig. 3. (a) Configuration of the DCB test specimen and (b) specimen under testing**.**

2.3.2. Mode II testing

The ENF test was conducted to determine the mode II interlaminar fracture toughness (G_{IIC}). The three-point bend fixture was used to perform this test with a span length of 76 mm [46]. The ENF specimen was prepared in 120×20 mm size. Fig. 4 shows the geometry of the ENF specimen and a picture for specimen during testing. The specimens were designed that (a/L) is 0.5 at the crack propagation. Controlling displacement was applied with a loading rate of 1 mm/min [43-44]. During the test the ENF specimen creates shear stress at the crack tip. When the crack propagation starts, the load suddenly dropped and the specimen failed. The direct beam theory was adopted for determining G_{IIC} using the equation below [43–48]:

$$G_{IIC} = \frac{9P\delta a^2}{2b(2L^3+3a^3)} \quad (4)$$

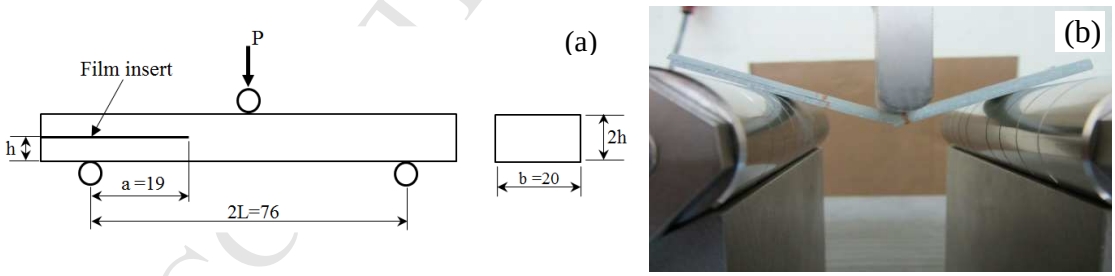

Fig. 4. (a) Geometry of the ENF specimen and (b) specimen under testing.

2.3.3. Tensile and flexural testing

Tensile and flexural test samples were prepared according to the ASTM D 638 in size of 165 × 13 mm for a gauge length of 50 mm and ASTM D 790 in size of 185 × 12.7 mm with span to thickness ratio of 32:1, respectively. Thickness of the all specimens was about 3.35±0.25 mm. The crosshead speeds for tensile and flexural testing were 2 mm/min and 4 mm/min, respectively. At least three specimens were

tested for each GFRE composite and perlite-filled glass/epoxy (Pr-GFRE) composites and average values of the results were calculated.

3. Results and discussions

3.1. Mode I interlaminar fracture toughness

Fig. 5 shows the load-COD curves obtained by conducting DCB tests on specimens of GFRE composite toughened by different perlite weight fractions. The figure shows that, the GFRE and Pr-GFRE composites exhibit a linear load-COD behavior up to the crack initiation point, afterward these curves exhibited non-linear crack growth behavior. Furthermore, the gap is small between the non-linear point and maximum load point. Besides, the maximum load point increased by the addition of perlite to GFRE composite. However, the fracture behavior of DCB specimen was distinctly different after addition of perlite. Hence, the maximum load-COD of GFRE is about 23 N-78 mm, while for Pr-GFRE composites are about 25 N-71 mm, 31 N-71 mm, 29 N-75 mm and 26 N-73 mm, respectively when the perlite content changed from 1, 3, 5, to 10 wt%, as presented in Table 2.

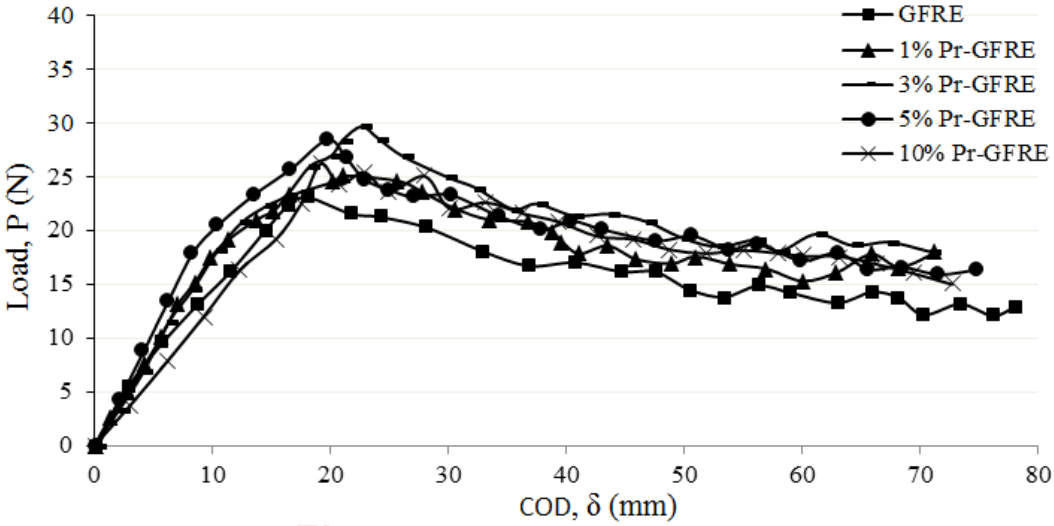

Fig. 5. Load-COD curves of the DCB tests for the GFRE and Pr-GFRE composites.

In details, when DCB test was conducted and the applied opening load reached near the maximum value, the delamination starts to propagate from the pre-crack tip (tip of the film insert) up to the delamination length reached 100 mm. Therefore, steady state crack growth behavior was observed such that insignificant rise and decrease of load values (zigzag) are noticed with respect to the displacement. Furthermore, the fracture onset represents the maximum load-COD value, which refers to the changing from the linear to nonlinear behavior in the load-COD curve. During the delamination extension, the bridged fibers were cracked or peel-off from the epoxy matrix and the separation of the both sides of the specimen increased, which this behavior explains the higher values of propagation fracture toughness (G_{IC}-Prop) than that of initiation fracture toughness (G_{IC}-Onset) values [48-51].

Table 2
Mode I interlaminar fracture toughness properties of the composites.

Composite type	Perlite content (wt%)	Maximum Load (N)	Maximum COD (mm)	G_{IC}-Onest (J/m^2)	G_{IC}-Onest increment (%)	G_{IC}-Prop (J/m^2)	G_{IC}-Prop increment (%)
GFRE	0	23.3 (±1.7)	78.1 (±3.9)	441 (±18)	-	615 (±27)	-
Pr-GFRE	1	25.1 (±1.5)	71.2 (±1.8)	490 (±19)	11.1	648 (±16)	5.4
	3	30.6 (±0.8)	70.7 (±1.6)	617 (±21)	39.9	706 (±24)	14.8
	5	28.5 (±1.4)	74.8 (±2.1)	540 (±17)	16.0	694 (±20)	12.8
	10	26.2 (±1.2)	72.7 (±1.7)	502 (±25)	13.8	674 (±31)	9.6

Resistance curves (R-curves) for the composites are presented in Fig.6. These curves demonstrate the variation of G_{IC} versus delamination length of the GFRE and Pr-GFRE composites. The values of G_{IC}-Onset and G_{IC}-Prop were defined according to the ASTM D-5528 standards, that G_{IC}-Onset at the maximum load point and G_{IC}-Prop corresponding to the average propagation values after maximum G_{IC} value of the R-curves.

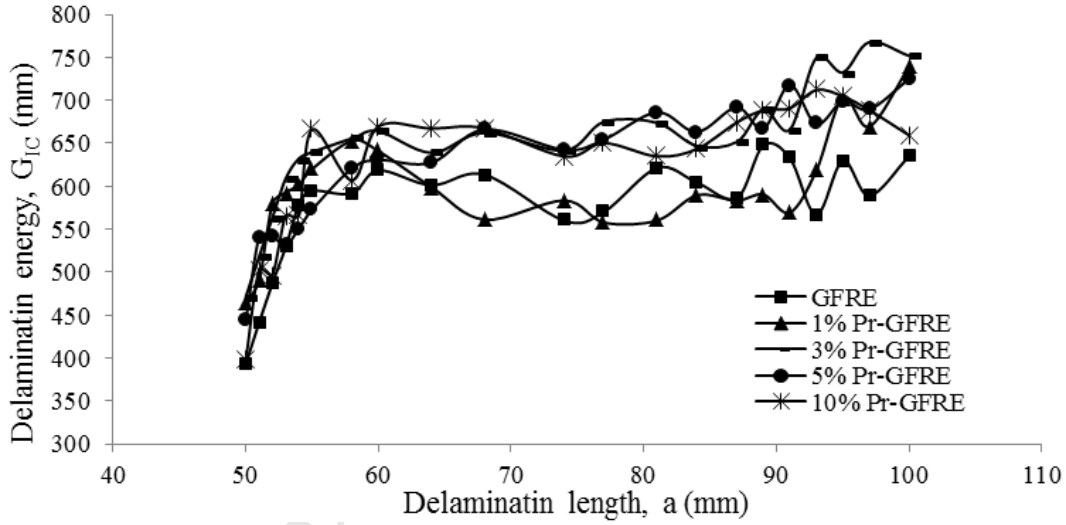

Fig. 6. R-curves for the GFRE and Pr-GFRE composites.

As illustrated in Fig. 7, G_{IC}-Onset and G_{IC}-Prop are enhanced with addition of perlite in GFRE laminates. Hence, the G_{IC}-Onset of GFRE composite was 441 J/m^2. When the perlite content increased from 1 wt% to 3 wt%, the G_{IC}-Onset increased from 490 J/m^2 to 617 J/m^2, then decreased to 502 J/m^2 at particle content of 10 wt%. Therefore, the G_{IC}-Onset increased by 11.1%, 39.9%, 16.0% and 13.8%, respectively compared with GFRE composite. The G_{IC}-Prop of GFRE composite was 615 J/m^2. When the perlite content increased from 1 to 3 wt%, the G_{IC}-Prop increased from 648 J/m^2 to 706 J/m^2, then decreased to 674 J/m^2 at perlite content of 10 wt%. The G_{IC}-Prop increased by 4.9%, 12.4%, 33.8% and 26.9%, respectively compared with that of GFRE composite. These slight drop in G_{IC}-Prop values can be described to the negative effects of void content and particle aggregation on the adhesion strength between perlite particles and matrix, which they act as stress concentration points and weakened the composite [3, 13, 52].

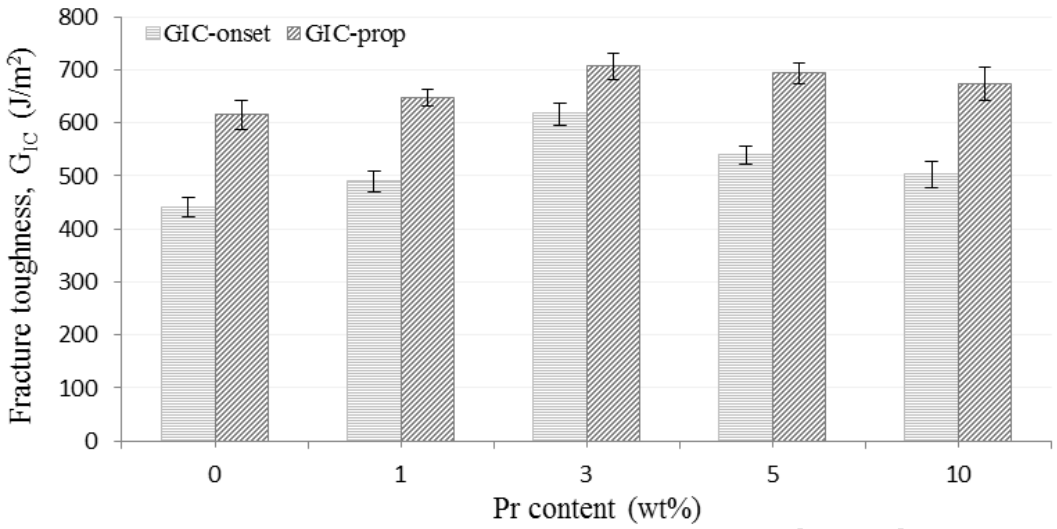

Fig. 7. Comparison of mode I interlaminar toughness values for the GFRE and Pr-GFRE composites.

3.2. Mechanisms of mode I interlaminar toughness

Fig. 8 depicts cross-section images of DCB specimens observed by optical microscope for the GFRE and 3 wt% Pr-GFRE composites. The cross-section images were selected at a place near the crack initiation point (Fig. 8a and c) and the final stage of crack propagation (Fig. 8b and d). For the GFRE specimen, the interlayer crack is straight, as shown in Fig. 8a. Moreover, some fiber bundles of GFRE specimen are pulled and broken out during the crack propagation, as presented in Fig. 8b. Hence, For the Pr-GFRE specimen (Fig. 8c and d), the interlayer crack is not straight (kinked crack path) and has rougher surface [3], therefore the fracture area increased compared with GFRE specimen. Accordingly, the crack propagation in Pr-GFRE specimen started later than that in the GFRE specimen.

As shown in Fig.9a the SEM image of the GFRE specimen fracture surface showed the glass fibers covered with the epoxy matrix and there are no pull out fibers. On the other hand, for the perlite particles filled GFRE composites (Fig.9b), the Pr particles were bonded with matrix and settled around the glass fibers that lead to microcrack bridging, thus the microcracking occurs in the epoxy matrix around the particles [3]. In addition, some of the plain woven glass fibers were pulled out from fracture surface, therefore the glass woven fibers provide also a bridging reinforcement. Therefore, the opening mode I energy was dissipated in the fiber/microcrack bridged zone near the crack tip. This behavior proved the chemical compatibility of Pr particles with glass fiber/epoxy system.

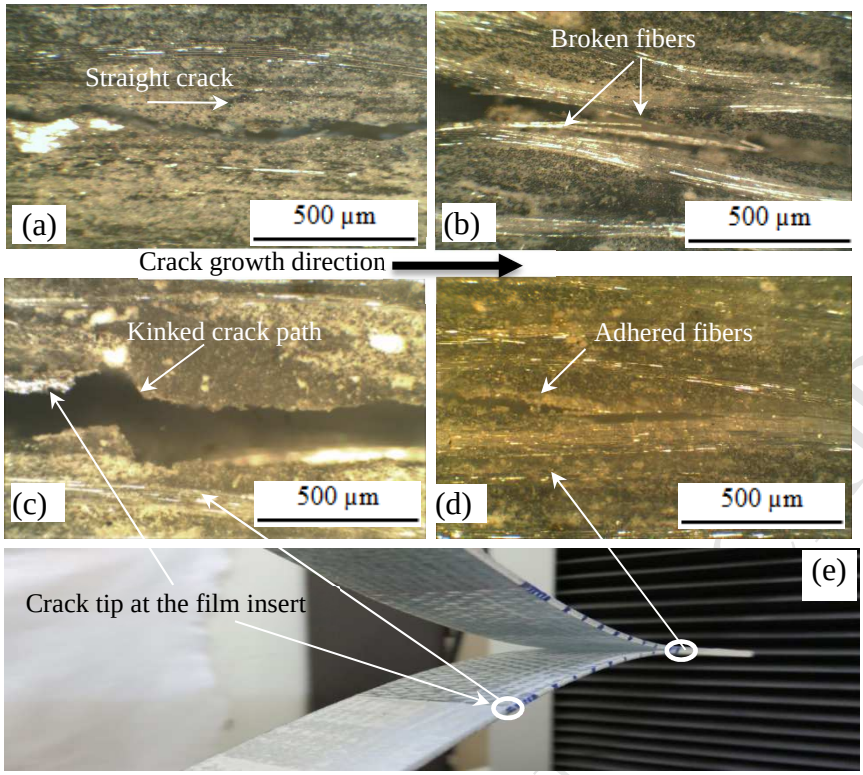

Fig. 8. The optical microscope images of DCB specimen for GFRE: (a) Crack near the film insert, (b) At the end of crack propagation, and for 3 wt% Pr-GFRE: (c) Crack near the film insert, (d) At the end of crack propagation and (e) The specimen.

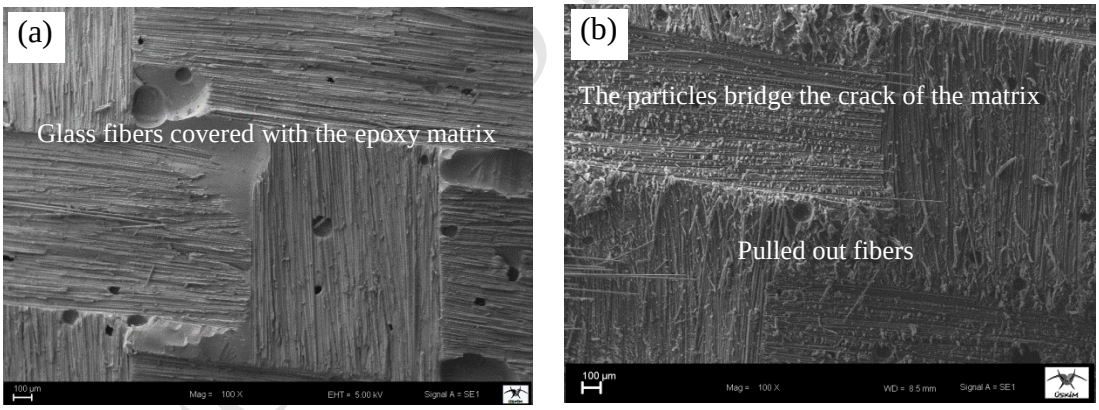

Fig. 9. SEM micrographs of mode I fracture surfaces of DCB specimens for: (a) GFRE, (b) 3 wt% Pr-GFRE composites.

3.3. Mode II interlaminar fracture toughness

Fig. 10 shows the representative load-displacement curves obtained by conducting ENF tests. As can be seen in figure, the GFRE and Pr-GFRE composites show a linear load–displacement behavior up to the point of crack initiation, afterwards load suddenly decreased and caused the unstable crack propagation and fracture. This behavior is affected by the brittle nature of epoxy resin. Moreover, there is a plateau

at the highest load. Therefore, the crack propagation was delayed by perlite particles [13, 51].

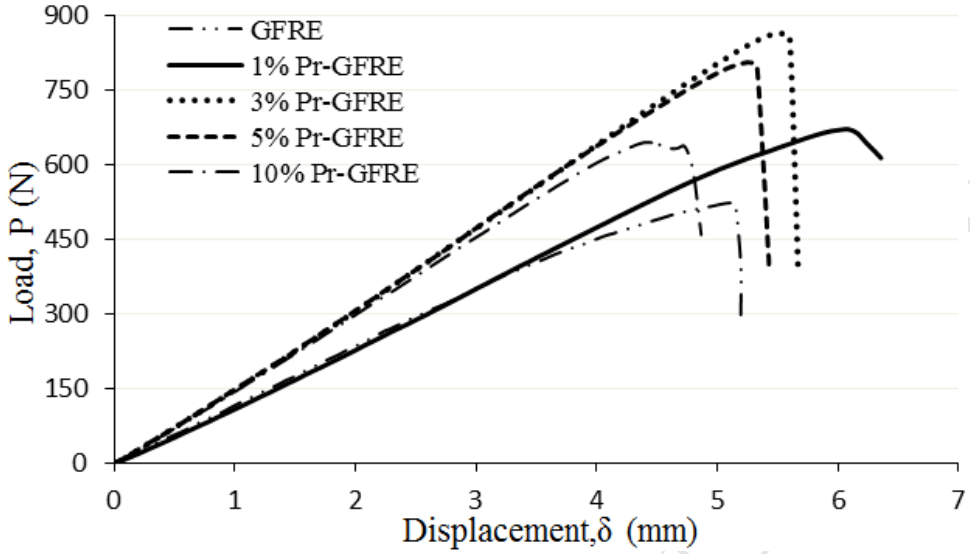

Fig. 10. Load-displacement curves of the ENF tests for the GFRE and Pr-GFRE composites.

For the GFRE composite, the maximum load and displacement values were about 522 N and 5.1 mm, respectively. On the other hand, after perlite addition, the maximum load increased gradually with increasing perlite content. Hence, the maximum load-displacement values for Pr-GFRE composites were about 670 N-6.1 mm, 863 N-5.5 mm, 804 N-5.3 mm and 644 N-4.5 mm, when the perlite content changed from 1, 3, 5, to 10 wt%, respectively. The detailed results are given in Table 3. When the content increased from 3 to 10 wt%, the displacement corresponding to the maximum load decreased from 5.51 mm to 4.45 mm.

Table 3
Mode II interlaminar fracture toughness properties of the composites.

Composite type	Perlite content (wt%)	Maximum Load (N)	Displacement at maximum load (mm)	Fracture toughness G_{IIC} (J/m^2)	G_{IIC} increment (%)
GFRE	0	522 (±22)	5.08 (±0.12)	1720 (±66)	-
Pr-GFRE	1	670 (±16)	6.09 (±0.18)	2544 (±43)	48.0
	3	863 (±23)	5.51 (±0.07)	2964 (±75)	72.3
	5	804 (±19)	5.28 (±0.12)	2644 (±44)	53.8
	10	644 (±12)	4.45 (±0.15)	1786 (±35)	3.8

The G_{IIC} of the composites had the highest value of 2964 J/m^2 at perlite content of 3 wt% (Fig. 11). After that content, G_{IIC} dropped gradually up to content 10 wt% of perlite. Compared with that of GFRE composite, G_{IIC} of the Pr-GFRE increased by 48.0%, 72.3%, 53.8% and 3.8%, respectively.

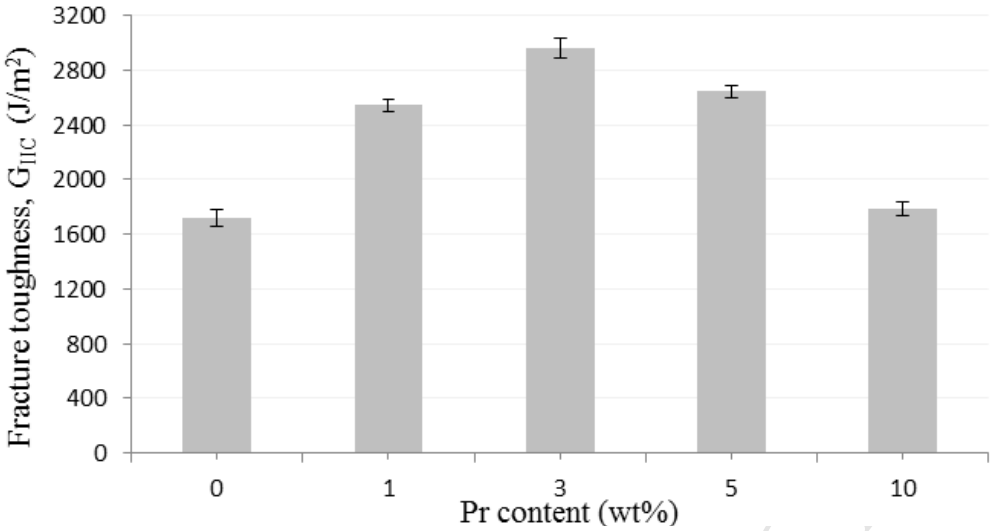

Fig. 11. Mode II interlaminar fracture toughness for the GFRE and Pr-GFRE composites.

3.4. Mechanisms of mode II interlaminar fracture toughness

The ENF specimen was applied to mode II loading creates maximum shear stress causes crack initiation and propagation in a form of crack moving from the crack tip at the film insert to mid-span of the specimen. The cross-section of the specimens was inspected by optical microscope for the GFRE and Pr-GFRE composites (Fig. 12(a) and (b)) at a place near the crack tip point. As shown in Fig. 12(a), the glass fibers are exposed during crack propagation between the surface of the fabric material and the matrix, while Fig. 12(b) illustrates the plastically deformed zones keep good adhesion for perlite particle/fiber/epoxy system. Chai [53, 54] introduced similar procedure for presenting the plastic shear deformation, which is the main parameter in controlling mode II interlaminar toughness.

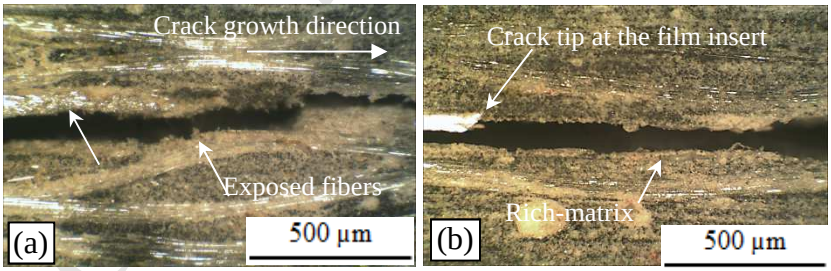

Fig. 12. The optical microscope images of mode II specimen cross-section for: (a) GFRE, (b) 3 wt% Pr-GFRE composites (Crack near the film insert).

Fig. 13 demonstrates SEM images of the fracture surface for ENF specimens in order to clarify the mode II interlaminar toughness results. In general, the mode II fracture was brittle fracture. Nevertheless, the fracture surface was different after perlite addition at the ply of interlayer. As shown in the specimen fracture surfaces near the mid-span (Fig. 13 (a)) for the GFRE composite, the fibers were pulled out and broken. On the other hand, as observed in SEM images (Fig. 13 (b)), Fiber bridging did not happen under mode II fracture loading. However, the particles also

can bridge the crack path under ENF test. Unlike DCB specimens that showed continuous crack growth along the matrix/fiber interface, ENF specimens exhibited discontinuous crack growth by microcrack combination, which led to initiate many hackles on the fracture surface. In addition, hackles and friction are responsible for the energy absorption of mode II fracture [3, 51]. Therefore, the highest mode II delamination energy was obtained for 3 wt% Pr-GFRE composite specimens. Hence, the fracture surface contain many hackles can provide more toughening.

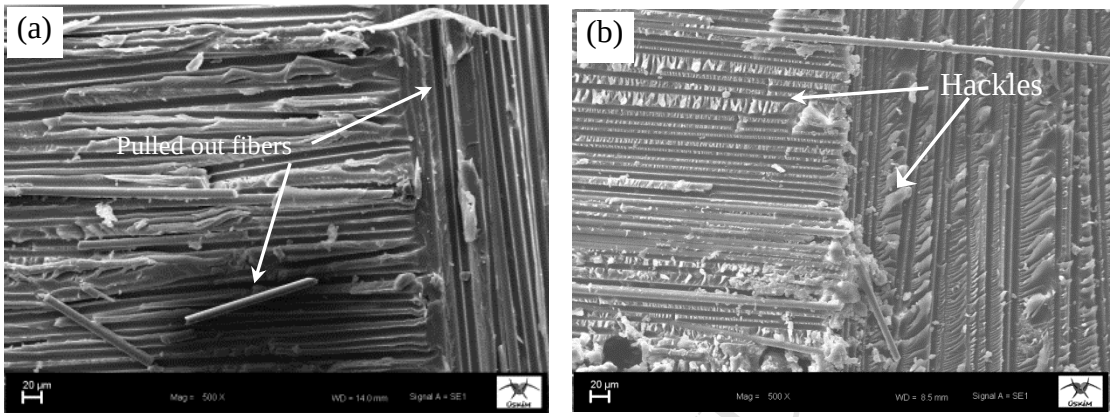

Fig. 13. The SEM micrographs of mode II interlaminar fracture surfaces for: (a) GFRE, (b) 3 wt% Pr-GFRE composites.

3.5. Effect of perlite contents on mechanical properties

Tensile strength and flexural properties of GFRE and Pr-GFRE composites are given in Table 4, also detailed investigations are illustrated in Fig. 14 and Fig.15. As shown in Fig. 14, the maximum tensile strength is 443 MPa at the perlite content of 1 wt% with maximum increment of 13.9%, compared with GFRE composite. Then, the composite tensile strength followed the trend of decreasing to reach 394 MPa at 10 wt% of perlite. The highest enhancement of flexural strength was obtained at perlite content of 5 wt% with maximum increment of 47.6%. In general, all the specimens of the Pr-GFRE composites have flexural strength higher than GFRE composite. For example, the flexural strength increased from 410 MPa to 605 MPa when the perlite content changed from 0 wt% to 5 wt%, then further increasing perlite particles, the flexural strength reduced to 553 MPa.

Table 4
Mechanical properties of the composites.

Composite type	Perlite content (wt%)	Tensile strength (MPa)	Flexural strength (MPa)	Failure strain (%)	Flexural modulus (MPa)
GFRE	0	389 (±09)	410 (±11)	2.08 (±0.05)	21.0 (±0.32)
Pr-GFRE	1	443 (±14)	559 (±18)	2.24 (±0.07)	22.9 (±0.17)
	3	432 (±11)	588 (±23)	2.43 (±0.08)	23.0 (±0.63)
	5	413 (±16)	605 (±13)	2.62 (±0.07)	22.2 (±0.29)
	10	379 (±12)	553 (±16)	2.59 (±0.09)	22.0 (±0.34)

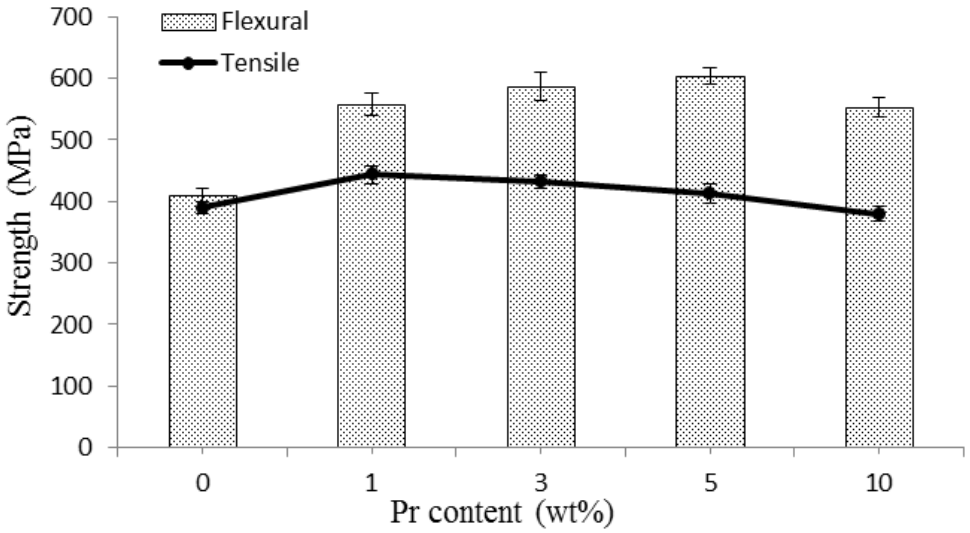

Fig. 14. Tensile and flexural strength versus perlite content for the GFRE and Pr-GFRE composites.

In principle, the failure strain values (Fig. 15) of the GFRE specimens moderately enhanced by adding perlite particles. Hence, the failure strain improved by 26.0% at perlite content of 5 wt%. Furthermore, the failure strain increased firstly from 2.08% for GFRE composite to 2.62% and then reduced to 2.59% at 10 wt% of perlite, which perhaps due to the higher modulus of rigid inorganic perlite particles than that of the polymer matrix. The flexural modulus of Pr-GFRE composites (Fig. 15) was slightly affected by addition of perlite, that the maximum modulus increased by 9.5% at perlite content of 3 wt%. While the flexural properties are degraded with thermoplastic filler addition, this strategy of using cheap industrial inorganic particles at least partly enhanced the mechanical properties.

As a result, the tensile and flexural experiments, perlite particles, added in GFRE composite, actually remarkably improved the flexural properties and tensile strength. The drop of the strength values may be attributed to the particle aggregation when the perlite content more than 5 wt%, forming weaknesses in the composite.

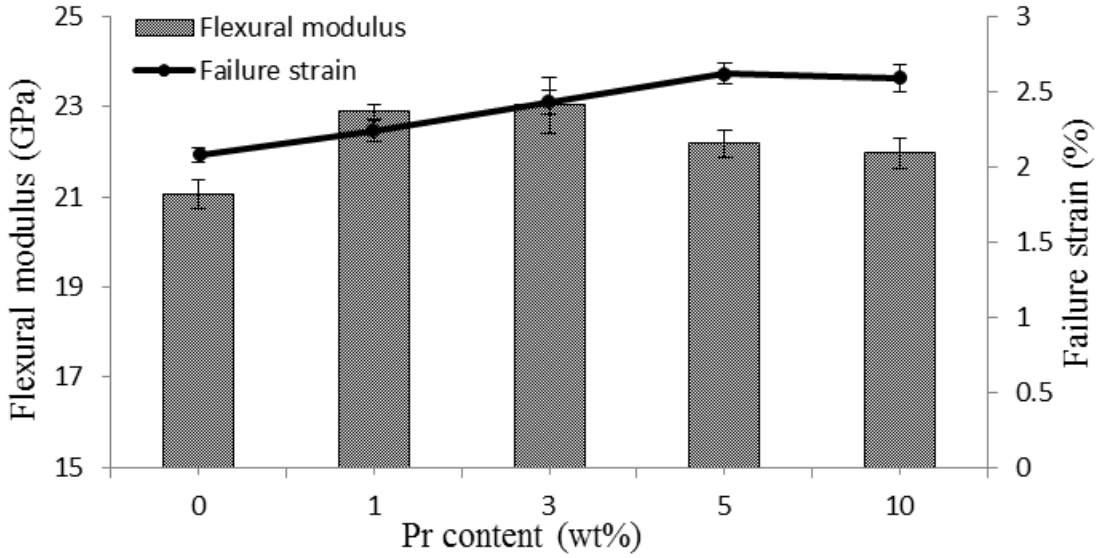

Fig. 15. Flexural modulus and failure strain versus perlite content for the GFRE and Pr-GFRE composites.

4. Conclusions

GFRE composites were manufactured with inclusion micro-perlite filler. The DCB, ENF, tensile and flexural tests were carried out according to ASTM standards. The main conclusions from this work can be summarized as follows:

- The addition of perlite particles with four different weight fractions to GFRE composite significantly improved the interlaminar fracture toughness for mode I and mode II delamination, tensile and flexural strength, flexural modulus and failure strain.
- The load-COD curves of DCB specimens were distinctly different after particle addition. Hence, the maximum load point increased and affected positively mode I interlaminar toughness.
- The initiation and propagation of mode I interlaminar fracture toughness, G_{IC}-Onset and G_{IC}-Prop were calculated from R-curves of DCB test, and their values are significantly increased by 39.9% and 14.8%, respectively, to reach maximum with perlite content of 3 wt%.
- The mode II interlaminar fracture toughness values were calculated from load-displacement data of ENF test that G_{IIC} was optimum at perlite content of 3 wt%, with maximum increment of 72.3%.
- The SEM and optical microscope images proved the improvement of mode I and mode II interlaminar fracture toughness can mainly attribute to the high debonding resistance of the perlite particles from matrix, and thus crack growth delayed through specimens during the tests. This mechanism indicates the chemical compatibility of the Pr-GFRE composites system.
- The tensile strength, flexural strength and flexural modulus reached highest values at perlite content of 1, 5 and 3 wt% with maximum increment of 13.9%, 47.6% and 9.5%, respectively.

References

[1] Erden S, Sever K, Seki Y, et al. Enhancement of the mechanical properties of glass/polyester composites via matrix modification glass/polyester composite siloxane matrix modification. Fibers Polym 2010;11:732–37.
[2] Sathishkumar TP, Satheeshkumar S, Naveen J. Glass fiber-reinforced polymer composites – a review. J Reinf Plast Comp 2014;33(13):1258–75.
[3] Srivastava VK, Hogg P J. Damage performance of particles filled quasi-isotropic glass-fibre reinforced polyester resin composites. J Mater Sci 1998;33:1119–28.
[4] Song MC, Sankar BV, Subhash G, Yen CF. Analysis of mode I delamination of zpinned composites using a non-dimensional analytical model. Compos Part B–Eng 2012; 43(4):1776–84.
[5] Mouritz AP, Koh TM. Re-evaluation of mode I bridging traction modeling for z-pinned laminates based on experimental analysis. Compos Part B–Eng 2014;56:797–807.
[6] Pegorin F, Pingkarawat K, Daynes S, Mouritz AP. Influence of z-pin length on the delamination fracture toughness and fatigue resistance of pinned composites. Compos Part B–Eng 2015;78:298–307.
[7] Mouritz AP, Cox BN. A mechanistic approach to the properties of stitched laminates. Compos Part A–Appl S 2000;31(1):1–27.

[8] Mall S, Katwyk DW, Bolick RL, Kelkar AD, Davis DC. Tension-compression fatigue behavior of a H-VARTM manufactured unnotched and notched carbon/ epoxy composite. Compos Struct 2009;90(2):201-7.

[9] Hameed N, Sreekumar PA, Francis B, et al. Morphology, dynamic mechanical and thermal studies on poly (styrene-co-acrylonitrile) modified epoxy resin/glass fibre composites. Compos Part A 2007;38:2422–32.

[10] Mezzenga R, Boogh L, Månson J-AE. A review of dendritic hyperbranched polymer as modifiers in epoxy composites. Compos Sci Technol 2001;61(5):787–95.

[11] Van der Heijden S, Daelemans L, De Schoenmaker B, De Baere L, Rachier H, Van Paepegem W, et al. interlaminar toughening of resin transfer moulded glass fibre epoxy laminates by polycaprolactone electrospun nanofibres. Compos Sci Technol 2014;104(19):66–73.

[12] Dadfar MR, Ghadami F. Effect of rubber modification on fracture toughness properties of glass reinforced hot cured epoxy composites. Mater Des 2013;47(0):16–20.

[13] Wang Z, Huang X, Bai L, Du R, Liu Y, Zhang Y, Zaho G. Effect of micro-Al_2O_3 contents on mechanical property of carbon fiber reinforced epoxy matrix composites. Compos Part B-Eng 2016;91:392–98.

[14] Tang YH, Ye L, Zhang DH, Deng SQ. Characterization of transverse tensile, interlaminar shear and interlaminate fracture in CF/EP laminates with 10 wt% and 20 wt% silica nanoparticles in matrix resins. Compos Part A–Appl S 2011; 42(12):1943–50.

[15] Fan Z, Santare MH, Advani SG. Interlaminar shear strength of glass fiber reinforced epoxy composites enhanced with multi-walled carbon nanotubes. Compos Part A–Appl S 2008;39(3):540–54.

[16] Zhu J, Imam A, Crane R, Lozano K, Khabashesku VN, Barrera EV. Processing a glass fiber reinforced vinyl ester composite with nanotube enhancement of interlaminar shear strength. Compos Sci Technol 2007;67(7–8):1509–17.

[17] Wang K, Cheng L, Wu JS, Toh ML, He CB, Yee AF. Epoxy Nanocomposites with highly exfoliated clay: mechanical properties and fracture mechanisms. Macromolecules 2005; 38:788–800.

[18] Tang Y, Ye L, Zhang Z, Friedrich K. Interlaminar fracture toughness and CAI strength of fibre-reinforced composites with nanoparticles – A review. Composites Science and Technology; 2013;86:26–37.

[19] Wang WX, Takao Y, Matsubara T, Kim HS. Improvement of the interlaminar fracture toughness of composite laminates by whisker reinforced interlamination. Compos Sci Technol 2002;62(6):767–74.

[20] Jen M-HR, Tseng Y-C, Wu C-H. Manufacturing and mechanical response of nanocomposite laminates. Compos Sci Technol 2005; 65(5):775–79.

[21] Gardea F, Lagoudas DC. Characterization of electrical and thermal properties of carbon nanotube/epoxy composites. Compos Part B-Eng 2014; 56:611–20.

[22] Jiang Q, Wang X, Zhu Y, Hui D, Qiu Y. Mechanical, electrical and thermal properties of aligned carbon nanotube/polyimide composites. Compos Part B–Eng 2014;56:408–12.

[23] Shiu S-C, Tsai J-L. Characterizing thermal and mechanical properties of graphene/epoxy. nanocomposites. Compos Part B–Eng 2014;56: 691–7.

[24] Chen Q, Wu W, Zhao Y, Xi M, Xu T, Fong H. Nano-epoxy resins containing electrospun carbon nanofibers and the resulting hybrid multi-scale composites. Compos Part B-Eng 2014;58:43–53.

[25] Bulut M. Mechanical characterization of basalt/epoxy composite laminates containing grapheme nanopellets. Compos Part B-Eng , 2017.
[26] Zabihi O, Ahmadi M, Nikafshar S, Preyeswary KC, Naebe M. A technical review on epoxy-clay nanocomposites: Structure, properties, and their applications in fiber reinforced composites. Compos Part B-Eng . 2017 Sep 30.
[27] Tarfaoui M, El Moumen A, Lafdi K. Progressive damage modeling in carbon fibers/carbon nanotubes reinforced polymer composites. Compos Part B-Eng . 2017 Mar 1;112:185-95.
[28] Kostagiannakopoulou C, Tsilimigkra X, Sotiriadis G, Kostopoulos V. Synergy effect of carbon nano-fillers on the fracture toughness of structural composites. Compos Part B-Eng . 2017 Nov 15;129:18-25.
[29] Landowski M, Strugała G, Budzik M, Imielińska K. Impact damage in SiO_2 nanoparticle enhanced epoxy–Carbon fibre composites. Compos Part B-Eng . 2017 Mar 15;113:91-9.
[30] Kumar A, Roy S. Characterization of mixed mode fracture properties of nanographene reinforced epoxy and Mode I delamination of its carbon fiber composite. Compos Part B-Eng . 2017 Sep 28.
[31] Ozdemir NG, Zhang T, Hadavinia H, Aspin I, Scarpa F. Glass fibre reinforced polymer composites toughened with acrylonitrile butadiene nanorubber. Composites Part B: Engineering. 2016 Mar 1;88:182-8.
[32] Demirci MT, Tarakçıoğlu N, Avcı A, Akdemir A, Demirci İ. Fracture toughness (Mode I) characterization of SiO_2 nanoparticle filled basalt/epoxy filament wound composite ring with split-disk test method. Compos Part B-Eng . 2017 Jun 15;119:114-24.
[33] El Moumen A, Tarfaoui M, Lafdi K, Benyahia H. Dynamic properties of carbon nanotubes reinforced carbon fibers/epoxy textile composites under low velocity impact. Compos Part B-Eng . 2017 May 23.
[34] Gupta N, Barar BS, Woldesenbet E. Effect of filler addition on the compressive and impact properties of glass fibre reinforced epoxy. Bull Mater Sci 2001;24: 219–23.
[35] Chung D.D.L. Composite Materials; Science and Applications. 2nd Ed. P.B. Derby, London: Springer-Verlag 2010.
[36] Perlite Institute .Perlite in Industry. https://www.perlite.org/industry/industrial-perlite.html. consulted 1 July 2016.
[37] Akın-Öktem G and Tinçer T. Preparation and Characterization of Perlite Filled High Density Polyethylenes. Part I. Mechanical Properties. J. of Applied Polymer Science 1994;54:1103-14.
[38] Akın-Öktem G and Tinçer T. A study on the yield stress of perlite-filled high-density Polyethylenes. J. of Materials Science 1993;28:6313-17.
[39] Akın-Öktem G, Tanrisinibilir S, Tinçer T. Study on mechanical properties of Perlite-Filled Gamma Irradiated Polypropylene. J. of Applied Polymer Science 2001;81:2670-78.
[40] Sahraeian R, Esfandeh M, Hashemi SA. Rheological, Thermal and Dynamic Mechanical Studies of the LDPE/Perlite Nanocomposites. Polymers& polymer composite 2013;21 (4):243-249.
[41] D Shastri, HS Kim. A new consolidation process for expanded perlite particles. Construction and Building Materials. 2014; 60:1–7.
[42] ASTM Standard D 5528-94a, Test Method for Mode I Interlaminar Fracture Toughness of Unidirectional Fiber-Reinforced Polymer Matrix Composites, American Society for Testing and Materials, West Conshohocken, PA, 2001.

[43] Albertsen H, Ivens J, Peters P, Wevers M, Verpoest I. Interlaminar fracture toughness of CFRP influenced by fiber surface treatment: Part 1 Experimental results. Compos Sci Technol 1995;54:133–45.
[44] Seyhan A, Tanoglu M, Schulte K, Mode I and mode II fracture toughness of E-glass non-crimp fabric/carbon nanotube (CNT) modified polymer based composites. Engng Fract Mech 2008;75:5151–62.
[45] Dharmawan F, Simpson G, Herszberg I, John S, Mixed mode fracture toughness of GFRP composites. Comps Struct 2006;75:328-38.
[46] Carlsson LA, Gillespie JW, Pipes RB. On the analysis and design of the end notched flexure (ENF) specimen for Model II testing. J Compos Mater 1986; 20:594-04.
[47] Lee JJ, Lim JO, Huh JS. Mode II interlaminar fracture behavior of carbon bead-filled epoxy/glass fiber hybrid composite. Polym Compos 2000; 21: 343–52.
[48] Srivastava V K, Hogg PJ. Moisture effects on the toughness, mode-I and mode-II of particles filled quasi-isotropic glass-fiber reinforced polyester resin composites. J Mater Sci 1998;33(5):1129-36.
[49] Lee SM. Mode II delamination failure mechanisms of polymer matrix composites. J Mater Sci 1997;32:1287–95.
[50] Wang T W, Daharani L R. Effect of interfacial mobility on flexural strength and fracture toughness of glass/epoxy laminates. J Mater Sci 1999;34:4873–82.
[51] Stevanovic D, Kalyanasundaram S, Lowe A, Jar P.-Y.B. Mode I and mode II delamination properties of glass/vinyl-ester composite toughened by particulate modified interlayers. Compos Sci Technol 2003;63:1949–64.
[52] Ning H, Weng S, Hu N, Yan C, Liu J, Yao J, Liu Y, Peng X, Fu S, Zhang J. Mode-II interlaminar fracture toughness of GFRP/Al laminates improved by surface modified VGCF interleaves. Compos Part B-Eng 2017;114:365-72.
[53] Chai H. Observation of deformation and damage at the tip of cracks in adhesive bonds in shear and assessment of a criterion for fracture. Int J Fract 1993;60:311–26.
[54] Chai H. Micromechanics of shear deformation in cracked bonded joints. Int J Fract 1992;58:223–39.